

## AGING EFFECT ON IONTOPHORETIC TRANSDERMAL DRUG DELIVERY

J.A. FERREIRA, P. DE OLIVEIRA AND L. PINTO

**ABSTRACT:** The skin is the largest organ of the human body offering an accessible interface for the administration of drugs. The main obstacle to transdermal drug delivery are the skin's barrier properties, due essentially to the stratum corneum, the skin outermost layer, that is impermeable to most drugs. There are several techniques used to modify the barrier properties of the stratum corneum and to enhance the permeation of drugs through the skin. One popular approach to overcome this barrier is iontophoresis, a technique where electric fields are applied to enhance the transport, by adding an electric potential gradient to a concentration gradient. Several factors affect iontophoresis assisted transdermal drug delivery (IATDD). Among them the mechanical properties of skin play an important role. The skin behaves like a viscoelastic material, and it is well known that transport in viscoelastic media is non-Fickian. Consequently, the traditional Fickian advection-diffusion iontophoretic models are inappropriate. As aging induces huge modifications in the mechanical properties of the skin, the models presented in this paper can provide clinicians with guidelines for personalized IATDD.

The paper is concerned with the analysis and numerical simulation of a non-Fickian viscoelastic model for iontophoretic transdermal drug transport. A multi-layer approach is followed, where the polymeric drug reservoir and the properties of the main skin layers are taken into account. Numerical simulations illustrate the effect of aging in TDD, and shed light on how to include it in personalized IATDD protocols.

**KEYWORDS:** Iontophoresis, Drug delivery, Skin, Aging, Viscoelasticity, Maxwell-Wiechert Model, Numerical Simulation.

### 1. Introduction

The skin is the largest organ of the human body and one of its most important functions is to protect the internal organs against external influences. Basically, it is composed by three layers: epidermis, dermis, and hypodermis. The stratum corneum is the outermost layer of the epidermis and has the important function of protecting the underlying tissue from chemical and mechanical stress. The second layer, the dermis, is the main layer of the skin and is mostly composed by elastin and collagen fibers. Just below the

epidermis-dermis interface is located the capillary bed that have an important role in systemic drug absorption. Loose fatty connective tissue is the main constituent of the hypodermis.

The skin has been used to deliver drugs in the systemic circulation as an alternative to oral or hypodermic administration. The main obstacle to transdermal drug delivery is the stratum corneum. This is either due to the low permeability of this layer or to the physio-chemical properties of the drug molecules. To increase drug transport and absorption, chemical and physical penetration enhancers have been used with great success. Chemical enhancers act by disrupting the skin barrier, thereby increasing transport by diffusion, while physical enhancers create a convective flow that can carry drug molecules.

A popular physical enhancer is low intensity, long duration electric current. This technique, known as iontophoresis, generates a potential gradient which induces a convective flow. More precisely two types of convective flows can be originated: one by the movement of charged drug molecules, and the other by the movement of interstitial fluid, a phenomenon known as electroosmosis. If high intensity, short duration electric fields are applied an increasing in the skin permeability can also be achieved. This technique is known as electroporation. In this paper we focus in iontophoretic transdermal drug delivery from a polymeric reservoir.

The skin is a viscoelastic tissue whose mechanical properties are mainly determined by collagen fibers, elastic fibers, and proteoglycans [6, 34, 32]. Aging has strong influence on these structures, which greatly affects the viscoelastic behavior of the skin. For instance, the elastin and collagen fibers tend to degenerate with age, which decreases the skin ability to recover from stress. Overall, these alterations induce an increase in the Young's modulus, particularly, in the stratum corneum and viable epidermis [24, 19, 7, 32]. Other aging related alterations in skin include decrease in hydration, atrophy of the capillary network, blood perfusion decrease, and decline in permeability [4, 7, 8, 22, 23, 32, 34, 36, 37]. There is a great controversy in the medical literature, concerning the impact of these modifications on the performance of TDA. Studies are conflicting in what concerns the effect of aging in the reduction of cutaneous blood perfusion that leads to a decrease on the systemic delivery; there is also controversy in what concerns the reduction of epidermal and dermal thicknesses and their influence in drug percutaneous penetration [23].

It is well known that drug transport in viscoelastic materials does not follow the classical Fick's law. To take into account the viscoelastic behavior, the drug flux  $J(t)$  should be expressed in terms of three main contributions:

$$J(t) = J_F(t) + J_{nF}(t) + J_{io}(t). \quad (1)$$

Here,  $J_{io}(t)$  denotes the convective mass flux due to the electric field, which is given by the Nernst-Planck relation (see for instance [18]). This flux can also include the interstitial convective flow induced by the charge of the medium. We recall that the human skin is negatively charged due to the presence of ionized carboxyle groups, therefore the interstitial fluid moves from the anode to the cathode. By  $J_F(t)$  and  $J_{nF}(t)$  we represent the Fickian and the non-Fickian flux, respectively. Here, we assume that  $J_{nF}(t) = D_v \nabla \sigma(t)$ , where  $\sigma(t)$  denotes the stress (the normal stress) and  $D_v$  represents the stress-driven tensor. For a detailed explanation of the form assumed for  $J_{nF}(t)$  see [13]. The functional dependence of the stress  $\sigma(t)$  on the strain  $\epsilon(t)$  depends on the viscoelastic properties of the medium. As mentioned before, the skin viscoelastic properties change with age. Then, it is of crucial importance to know how aging affects drug absorption.

Mathematical modeling of iontophoretic transdermal drug delivery aims to study the drug absorption in the blood stream in function of the iontophoretic protocol and skin characteristics. Without being exhaustive, we mention the papers [35], [28], and [29] that are devoted to the mathematical modeling of iontophoretic/electroporated transdermal drug delivery systems. In these papers the mathematical description is centered in the passive diffusion, convective transport induced by the electric field, and electroosmosis induced by the fluid flow generated in charged porous membranes like the skin. Recently, in [14], the qualitative behavior of drug release from a polymeric reservoir and absorption in the blood stream is studied in function of iontophoresis protocols. The analysis of the discrete model is also established. In [30], a one-dimensional multilayered model for iontophoretic transdermal drug delivery from a polymeric reservoir was considered. The qualitative properties were analytically and numerically studied. When high intensity electric fields are applied in the skin, the temperature increases, which also influences drug transport. Mathematical models that also take into account the temperature evolution were considered for instance in [3], [1], and [2].

In this work, our aim is to describe mathematically the drug transport through the skin and its absorption when the skin viscoelastic nature is taken

into account. To circumvent the opposition represented by an increased stiffness, and namely to take into account aging effects, we consider IATDD. The model describes the release from a polymeric reservoir and its transport through the skin until the capillary bed where it enters the blood stream. The drug transport in the viscoelastic skin is coupled with the potential generated by an iontophoretic protocol. We consider a multilayered model composed by the polymeric reservoir, the stratum corneum, the so called viable epidermis, and the dermis bounded by the capillaries. The novelty of the present paper is that the model takes into account the viscoelastic behavior of the skin layers. The drug transport is described by integro-differential equations that are established combining mass conservation law with a generalized flux defined in equation (1). Such integro-differential equations are derived considering that the viscoelastic behavior of the skin layers are described by Maxwell-Wiechert models ([5, 12]). To complete the description of the drug transport we consider adequate initial and boundary conditions, as well as proper interface conditions that describe drug transport between skin layers. Since we are dealing with iontophoretic transdermal drug delivery, the convective velocity is defined by Nernst-Planck equation that depends on the gradient of the electric potential. This potential is defined by spatial coupled Poisson's equations combined with convenient interface and boundary conditions (see for instance [3]).

To solve the advection dominated non-Fickian viscoelastic transport model we use a finite difference scheme based on the so called method of lines approach: a spatial discretization followed by a time integration. The spatial discretization is defined discretizing the advection term by a weighted essentially non-oscillatory (WENO) scheme while standard finite differences are used for the other terms. For the time discretization we use an implicit-explicit (IMEX) multistep method, where the non-stiff advective term is treated explicitly and the other terms are treated implicitly. The proposed method takes into account possible discontinuities in the functions coefficients. For the elliptic electroporation model the analytical solution can be easily obtained.

The paper is organized as follows. In Section 2 we derive the mathematical model. Next, in Section 3, we establish energy estimates that can be used to explain the role of the parameter models in the drug absorption phenomenon. The stability of the coupled model is also concluded. The numerical scheme is presented in Section 4. Numerical experiments illustrating the theoretical

results and the qualitative behaviour of the model are included in Section 5. We finish with some conclusions in Section 6.

## 2. Iontophoretic drug transport in viscoelastic tissues

Let us consider a polymeric reservoir in contact with the skin where, due to the different viscoelastic properties, we distinguish three layers: the stratum corneum, the viable epidermis, and the dermis. To simplify, the polymeric matrix and the skin layers are assumed homogeneous and isotropic. These assumptions allow the replacement of the three dimensional physical domain by the one dimensional domain  $\Omega = [-L_{dp}, L_s]$ , where  $L_{dp}$  and  $L_s$  denote the length of the drug patch (dp) and of the skin layer (s), respectively. We assume that the interface between the drug patch and the skin is located at  $x = 0$  and we represent by  $L_{sc}$ ,  $L_e$ , and  $L_d$ , the thickness of the stratum corneum (*sc*), viable epidermis (*e*), and dermis (*d*), i.e,  $L_s = L_{sc} + L_e + L_d$ . To simplify we also use the following notation:  $\Omega_{dp} = (-L_{dp}, 0)$ ,  $\Omega_{sc} = (0, L_{sc})$ ,  $\Omega_e = (L_{sc}, L_{sc} + L_e)$ , and  $\Omega_d = (L_{sc} + L_e, L_s)$ .

We assume that initially an amount of ionized drug is uniformly dispersed in the polymeric reservoir and that two electrodes are present on the left and right parts of the domain, i.e., one in contact with the polymeric matrix and the other in contact with the dermis. The electrode in contact with the polymeric matrix has the same charge of the drug and an electric potential is applied in both electrodes. This is a reasonable one dimensional approximation of transdermal electrical stimulation.

Let  $c_i(t)$ ,  $i = dp, sc, e, d$ , denote the concentration of an ionized drug with charge  $z_i$  depending on the spatial layer  $i$ . Let  $J_i(t)$ ,  $i = dp, sc, e, d$ , be the corresponding drug fluxes defined by (1). We assume that

$$J_{i,F}(t) = -D_{i,F} \nabla c_i(t), \quad (2)$$

where  $D_{i,F}$  denotes the drug diffusion coefficient in the layer  $i$ . We define

$$J_{i,nF}(t) = -D_{i,v} \nabla \sigma_i(t), \quad (3)$$

where  $D_{i,v}$  represents the stress-driven coefficient and  $\sigma_i(t)$  the stress developed by the viscoelastic layer  $i$ . The drug molecules stress the polymeric matrix, or the extracellular skin matrix. Responding to this stress such matrices exert a force opposite to the drug movement from regions of high stress to regions of lower stress according to (3).

Functional relations between the viscoelastic diffusion coefficient  $D_{i,v}$  and concentration  $c_i$  were constructed in [13]. In what follows we consider that

$D_{i,v}$  is constant. Drug delivery in viscoelastic materials was studied for instance in [9], [12], [13], and [10]. The viscoelastic behavior of the polymeric matrix and skin layers are described by the Boltzman integral

$$\sigma_i(t) = - \int_0^t E_i(t-s) \frac{\partial \epsilon_i}{\partial s}(s) ds, \quad (4)$$

where the modulus  $E_i(s)$  is given by the Maxwell-Wiechert model

$$E_i(s) = E_{i,0} + E_{i,1} e^{-\frac{s}{\tau_i}}. \quad (5)$$

In (5)  $E_{i,1}$  represents the Young's modulus of the Maxwell fluid arm and the relaxation times  $\tau_i$  are given by  $\tau_j = \mu_i/E_{1,i}$ . Here,  $\mu_i$  represents the viscosity and  $E_{i,0}$  stands for the Young's modulus of the free spring.

Assuming that  $\epsilon_i(t) = \alpha_i c_i(t)$ , from (4) we obtain

$$\sigma_i(t) = -\alpha_i(E_{i,0} + E_{i,1})c_i(t) + \alpha_i(E_{i,0} + E_{i,1}e^{-\frac{t}{\tau_i}})c_i(0) + \alpha_i \frac{E_{1,i}}{\tau_i} \int_0^t e^{-\frac{t-s}{\tau_i}} c_i(s) ds$$

and consequently we get for  $J_{i,nF}(t)$  the following expression

$$J_{i,nF}(t) = -\alpha(E_{i,0} + E_{i,1})D_{i,v} \nabla c_i(t) + D_{i,v} \frac{E_{1,i}}{\tau_i} \alpha_i \int_0^t e^{-\frac{t-s}{\tau_i}} \nabla c_i(s) ds \quad (6)$$

provided that  $c_i(0)$  is constant in space. Then,  $J_{i,F}(t) + J_{i,nF}(t)$  is given by

$$J_{i,F}(t) + J_{i,nF}(t) = -\tilde{D}_{i,F} \nabla c_i(t) + \tilde{D}_{i,nF} \int_0^t e^{-\frac{t-s}{\tau_i}} \nabla c_i(s) ds, \quad (7)$$

where  $\tilde{D}_{i,F} = D_{i,F} - \alpha_i(E_{i,0} + E_{i,1})D_{i,v}$  and  $\tilde{D}_{i,nF} = D_{i,v} \alpha_i E_{i,1} / \tau_i$ , for  $i = dp, sc, e, d$ .

The convective flux induced by the iontophoretic electric field has two main contributions: electrical mobility due to the electric potential and electroosmosis. We set

$$J_{i,io}(t) = -v_{i,e} c_i(t) \pm v_{i,o} c_i(t) \quad (8)$$

where the electrophoretic mobility  $v_{i,e}$  is induced by electromigration, which is defined according to the Nernst-Planck equation

$$v_{i,e} = \frac{\tilde{D}_{i,F} \mathbf{e}_i z_i F}{RT}, \quad (9)$$

where  $\mathbf{e}_i$  denotes the electric field generated by the applied potential at the electrodes,  $F$  denotes the Farady constant,  $R$  is the gas constant, and  $T$  represents the absolute temperature. In (8),  $v_{i,o}$  denotes the flow velocity

caused by the electric potential where  $+$  or  $-$  is adopted depending on the direction of the flow:  $+$  ( $-$ ) if the direction of the flow is opposite (equal) to the direction of the electromigration. Finally,  $\tilde{D}_{i,F}$  is the diffusion coefficient of the Fickian part of the flux  $J_{i,F}(t) + J_{i,nF}(t)$  defined by (7).

In each layer  $\Omega_i$ , the drug transport is then described by the following integro-differential equation

$$\frac{\partial c_i}{\partial t} = \nabla \cdot (\tilde{D}_{i,F} \nabla c_i - \bar{v}_i c_i) + \int_0^t e^{-(t-s)/\tau_i} \nabla \cdot (\tilde{D}_{i,nF} \nabla c_i(s)) ds, \quad \text{in } \Omega_i \times (0, T], \quad (10)$$

where  $\bar{v}_i = -v_{i,e} \pm v_{i,o}$ , and  $i = dp, sc, e, d$ .

We observe that the complexity of the previous equation increases if we take into account other drug phenomena like degradation or binding. Moreover, if the drug in the polymeric matrix is assumed to be in the solid state then a dissolution process needs to be included in this model.

Regarding boundary conditions, we assume that the polymeric matrix is isolated, that is no flux occurs through the boundary  $-L_{dp}$ ,

$$J_{dp}(-L_{dp}, t) = 0, \quad t \in (0, T]. \quad (11)$$

We also assume that all the drug that enters in the capillaries is immediately removed from the system, that is

$$c_d(L_s, t) = 0, \quad t \in (0, T]. \quad (12)$$

To complete the description of the drug evolution we impose interface conditions at the contact points between the polymer and the stratum corneum ( $x = 0$ ), the stratum corneum and the viable epidermis ( $x = L_{sc}$ ), and the viable epidermis and the dermis ( $x = L_{sc} + L_e$ ). To simplify our analysis, which is oriented to understand the effect of skin viscoelasticity in iontophoretic drug transport, we assume continuity of concentration and mass flux, that is

$$\begin{aligned} J_{dp}(0, t) &= J_{sc}(0, t), & c_{dp}(0, t) &= c_{sc}(0, t), \\ J_{sc}(L_{sc}, t) &= J_e(L_{sc}, t), & c_{sc}(L_{sc}, t) &= c_e(L_{sc}, t), \\ J_e(L_{sc} + L_e, t) &= J_d(L_{sc} + L_e, t), & c_e(L_{sc} + L_e, t) &= c_e(L_{sc} + L_e, t). \end{aligned} \quad (13)$$

More realistic conditions would allow the discontinuity of the drug concentration at the interfaces. This can be achieved replacing conditions (13) by Kedem-Katchalsky type equations (see [30]).

To close the mathematical model we need to specify the initial conditions. We assume the following,

$$\begin{aligned} c_{dp}(0) &= c_0, \text{ in } \overline{\Omega}_{dp}, & c_{sc}(0) &= 0, \text{ in } \overline{\Omega}_{sc}, \\ c_e(0) &= 0, \text{ in } \overline{\Omega}_e, & \text{and } c_d(0) &= 0, \text{ in } \overline{\Omega}_d. \end{aligned} \quad (14)$$

Moreover, we still need to define the electric field  $\mathbf{e}_i$  in the electrophoretic mobility (9). Since the electric field is given by the gradient of the potential,  $\mathbf{e}_i = \nabla\phi_i$  and as each skin layer is electrically neutral [18], the potential is governed by the Laplace equation

$$-\nabla \cdot (\psi_i \nabla \phi_i) = 0, \quad \text{in } \Omega_i, \quad i = dp, sc, e, d. \quad (15)$$

In equation (15)  $\phi_i$  and  $\psi_i$  denote the potential and the electric conductivity at the several layers ( $i = dp, sc, e, d$ ). We complement equation (15) with the following boundary conditions

$$\phi = v_0, \quad \text{at } x = -L_{dp}, \quad (16)$$

at the anode and

$$\phi = 0, \quad \text{at } x = L_s, \quad (17)$$

at the cathode.

The flux and the potential continuity are imposed at each layer interface

$$\begin{aligned} \phi_{dp} &= \phi_{sc}, & \psi_{dp} \nabla \phi_{dp} &= \psi_{sc} \nabla \phi_{sc}, & \text{at } x &= 0 \\ \phi_{sc} &= \phi_e, & \psi_{sc} \nabla \phi_{sc} &= \psi_e \nabla \phi_e, & \text{at } x &= L_{sc} \\ \phi_e &= \phi_d, & \psi_e \nabla \phi_e &= \psi_d \nabla \phi_d, & \text{at } x &= L_{sc} + L_e. \end{aligned} \quad (18)$$

We observe that the potential interface conditions (18) can be replaced by conditions of type Kedem-Katchalsky (see [30]).

To close the model it is necessary to compute the electroosmotic velocity  $v_{i,o}(t)$ . The Navier-Stokes equations are usually used to describe  $v_{i,o}$  as in [17]. To maintain our model manageable, we neglect this velocity in what follows.

### 3. Energy estimates

**3.1. Electric field.** We start this section by establishing an upper bound for the electric field  $\mathbf{e}_i = \nabla\phi_i$ ,  $i = dp, sc, e, d$ . Let  $\hat{\phi} \in H^1(\Omega)$ , with  $\Omega = (-L_{dp}, L_s)$ ,

and such that  $\hat{\phi}(-L_{dp}) = \phi_0$  and  $\hat{\phi}(L_s) = 0$ . We note that the simplest function satisfying the previous assumption is

$$\hat{\phi}(x) = \phi_0 - \frac{x + L_{dp}}{L_{dp} + L_s}, \quad x \in \bar{\Omega}.$$

It is easy to show the following inequality,

$$\sum_{i=dp,sc,e,d} (\psi_{i,min} - \epsilon^2) \|\nabla(\phi_i - \hat{\phi})\|_{L^2(\Omega_i)}^2 \leq \frac{1}{4\epsilon^2} \|\nabla\hat{\phi}\|_{L^2(\Omega)}^2 \sum_{i=dp,sc,e,d} \psi_{i,max}^2, \quad (19)$$

where  $\epsilon \neq 0$  and

$$\psi_{i,min} = \min_{\bar{\Omega}_i} \psi_i, \quad \psi_{i,max}^2 = \max_{\bar{\Omega}_i} \psi_i.$$

To establish inequality (19) we need to assume that  $\phi_i \in H^1(\Omega_i)$ ,  $i = dp, sc, e, d$ ,

For  $\epsilon$  such that  $\epsilon^2 < \psi_{i,min}$ ,  $i = dp, sc, e, d$ , we get

$$\sum_{i=dp,sc,e,d} \|\nabla(\phi_i - \hat{\phi})\|_{L^2(\Omega_i)}^2 \leq \frac{1}{\epsilon^2} \|\nabla\hat{\phi}\|_{L^2(\Omega)}^2 \frac{\max_{i=dp,sc,e,d} \psi_{i,max}^2}{\min_{i=dp,sc,e,d} \psi_{i,min} - \epsilon^2} \quad (20)$$

and then

$$\sum_{i=dp,sc,e,d} \|\nabla\phi_i\|_{L^2(\Omega_i)}^2 \leq \left(1 + \frac{1}{\epsilon^2} \frac{\max_{i=dp,sc,e,d} \psi_{i,max}^2}{\min_{i=dp,sc,e,d} \psi_{i,min} - \epsilon^2}\right) \|\nabla\hat{\phi}\|_{L^2(\Omega)}^2 \quad (21)$$

The solution of the elliptic problem (15) that defines electric potential is solved analytically [30]. Consequently, in what follows we assume that the velocities  $\bar{v}_i$ ,  $i = dp, sc, e, d$ , are known functions.

**3.2. Drug concentration.** Next, we establish an upper bound for the drug concentration in  $\Omega$ . We assume that the function describing the drug concentration is in  $H_0^1(\Omega)$ . It is easy to show that we have

$$\frac{1}{2} \frac{d}{dt} \|c_i(t)\|_{L^2(\Omega_i)}^2 + J_i(\Omega_i^+) c_i(\Omega_i^+) \eta_i^+ - J_i(\Omega_i^-) c_i(\Omega_i^-) \eta_i^- (J_i(t), \nabla c_i(t))_{L^2(\Omega_i)} = 0, \quad (22)$$

for  $i = dp, sc, e, d$ , where  $\Omega_i = (\Omega_i^-, \Omega_i^+)$ . Using the boundary and interface conditions (11), (12), (13), we get from equation (22)

$$\frac{1}{2} \sum_{i=dp,sc,e,d} \frac{d}{dt} \|c_i(t)\|_{L^2(\Omega_i)}^2 - \sum_{i=dp,sc,e,d} (J_i(t), \nabla c_i(t))_{L^2(\Omega_i)} = 0. \quad (23)$$

The last representation has an important role in the establishment of Proposition 1 whose proof can be seen in Section 7 (Appendix).

**Proposition 1.** *Let  $c \in L^2(0, T, H_0^1(\Omega))$  be the solution of the initial boundary value problem (10), (11), (12), (13), and (22) with the velocities  $\bar{v}_i, i = dp, sc, e, d$ , defined by the boundary value problem (15), (16), (17) and (18). If  $c \in C^1([0, T], L^2(\Omega))$ , then there exists a positive constant  $C_P$  such that if*

$$\min_{i=dp,sc,e,d} \tilde{D}_{iF} - C_P \max_{i=dp,sc,e,d} \|\bar{v}_i\|_{L^\infty(\Omega_i)} \geq 0. \quad (24)$$

we have

$$\begin{aligned} \sum_{i=dp,sc,e,d} \|c_i(t)\|_{L^2(\Omega_i)}^2 + \sum_{i=dp,sc,e,d} \tilde{D}_{i,nF} \left\| \int_0^t e^{-\frac{t-s}{\tau_i}} \nabla c_i(s) ds \right\|_{L^2(\Omega_i)}^2 \\ \leq e^{\gamma t} \|c_{dp}(0)\|_{L^2(\Omega_{dp})}^2, \quad t \in [0, T], \end{aligned} \quad (25)$$

where

$$\gamma = \max\left\{-\min_{i=dp,sc,e,d} \frac{2}{\tau_i}, -\frac{2}{C_P^2} \left( \min_{i=dp,sc,e,d} \tilde{D}_{iF} - C_P \max_{i=dp,sc,e,d} \|\bar{v}_i\|_{L^\infty(\Omega_i)} \right)\right\}. \quad (26)$$

■

The decreasing rate  $\gamma$  of

$$\sum_{i=dp,sc,e,d} \|c_i(t)\|_{L^2(\Omega_i)}^2 + \sum_{i=dp,sc,e,d} \tilde{D}_{i,nF} \int_0^t \|e^{-\frac{t-s}{\tau_i}} \nabla c_i(s)\|_{L^2(\Omega_i)}^2 ds$$

depends on the parameters that characterize the polymeric reservoir, the skin layers, the drug and the iontophoretic protocol. The estimate (25) was established under the condition (24) which means that the transport process is diffusion dominated.

The upper bound (25) is now used to obtain an upper bound for the drug mass  $M(t)$  in  $\Omega$ . In fact, we have

$$\begin{aligned} M(t) &= \sum_{i=dp,sc,e,d} \int_{\Omega_i} c_i(x, t) dx \\ &\leq \sqrt{L_{dp} + L_s} \left( \sum_{i=dp,sc,e,d} \|c_i(t)\|_{L^2(\Omega_i)}^2 \right)^{1/2}. \end{aligned} \quad (27)$$

Then from (25) we conclude

$$M(t) \leq \sqrt{L_{dp} + L_s} e^{\frac{1}{2}\gamma t} \|c_{dp}(0)\|_{L^2(\Omega_{dp})}, \quad t \in [0, T]. \quad (28)$$

We remark that estimate (28) is physically "sharp" in the sense that its second member exhibits a sound behavior. In fact:

- as the Young's modulus decrease, the decreasing rate  $\gamma$  also decreases and consequently we conclude that the upper bound for the drug mass contained in the polymer-skin system decreases;
- as the diffusion coefficients increase, the rate  $\gamma$  decreases that leads to a decreasing of the upper bound for the drug mass  $M(t)$ ;
- as the thickness of the skin layers decrease, decreases the upper bound for the drug mass in the polymer-skin system.

Following the approach in [14], estimate (28) can be used to get a lower bound for the absorbed drug mass  $M_{ab}(t) = M(0) - M(t)$ . In fact we have

$$M_{ab}(t) \geq M(0) - \sqrt{L_{dp} + L_s} e^{\frac{1}{2}\gamma t} \|c_{dp}(0)\|_{L^2(\Omega_{dp})}, t \in [0, T]. \quad (29)$$

The lower estimate for  $M_{ab}(t)$  is now used to characterize the time that the polymer-skin system takes to release a certain mass of drug. We have the following result:

**Proposition 2.** ([11]) *Let us suppose that the assumptions of Proposition 1 hold and let  $\epsilon > 0$  be a lower bound for the absorbed drug mass  $M_{ab}(t)$ ,  $\epsilon < M(0)$ , then  $M_{ab}(t) \geq \epsilon$ , for  $t \geq t^*$ , where  $t^*$  is given by*

$$t^* = \frac{\ln \left( \frac{M(0) - \epsilon}{\sqrt{L_s + L_{dp}} \|c_{dp}(0)\|_{L^2(\Omega_{dp})}} \right)}{\frac{1}{2}\gamma}. \quad (30)$$

and  $\gamma$  is defined by (26). ■

From (30) we conclude that  $t^*$  decreases if one of the following items holds

- the Young's modulus decrease;
- the diffusion coefficients increase;
- the thickness of the skin layers decreases.

The estimate in Proposition 1 implies the stability of the initial boundary value problem (10), (11), (12), (13), and (22) with the velocities  $\bar{v}_i, i = dp, sc, e, d$ , defined by the boundary value problem (15), (16), (17) and (18) in  $L^\infty(0, T, L^2(\Omega))$ . We can establish the same stability result with weaker regularity assumptions.

**Proposition 3.** *Let us suppose that the solution  $c_i, i = dp, sc, e, d$ , of the initial boundary value problem (10), (11), (12), (13), and (22) with the velocities  $\bar{v}_i, i = dp, sc, e, d$ , defined by the problem boundary value problem (15), (16), (17) and (18) is such that  $c_i \in C^1([0, T], L^2(\Omega_i)) \cap L^2(0, T, H^1(\Omega_i))$ ,  $i = dp, sc, e, d$ . Then*

$$\begin{aligned}
& \sum_{i=dp,sc,e,d} \|c_i(t)\|_{L^2(\Omega_i)}^2 + \sum_{i=dp,sc,e,d} \tilde{D}_{iF} \int_0^t \|\nabla c_i(s)\|_{L^2(\Omega_i)}^2 ds \\
& \quad + \sum_{i=dp,sc,e,d} \tilde{D}_{i,nF} \left\| \int_0^t e^{-\frac{t-s}{\tau_i}} \nabla c_i(s) ds \right\|_{L^2(\Omega_i)}^2 \\
& \leq e^{t \max_{i=dp,sc,e,d} \frac{\|\bar{v}_i\|_{L^\infty(\Omega_i)}^2}{\tilde{D}_{iF}}} \left( \|c_{dp}(0)\|_{L^2(\Omega_{dp})}^2 - 2\beta_{dp,sc} \int_0^t (c_{dp}(0, s) - c_{sc}(0, s))^2 ds \right),
\end{aligned} \tag{31}$$

for  $t \in [0, T]$ . ■

Inequality (31) leads to the stability of the coupled problem: diffusion problem (10), (11), (12), (13), and (22), elliptic problem (15), (16), (17) and (18). The uniqueness of the solution of the previous problem is also consequence of Proposition 3.

## 4. Numerical method

In this section we present a numerical scheme for the integro-differential equation (10). Our numerical procedure takes into account the dynamics of the drug transport process through the several skin layers. Note that for the elliptic equation (15) governing the electric potential we can obtain the exact solution [30].

When an electrical stimulus is applied, the convective field is the dominant process in the drug transport. In fact, the magnitude of the diffusion and viscoelastic diffusion coefficients in the several skin layers is very low, therefore, even for moderate potential values (e.g.,  $v_0 \geq 1V$ ), convective transport is more significant than diffusion like transport. In this case it is well known that traditional finite difference methods, e.g, based on centered approximations, can lead to non-physical oscillations near steep gradients or discontinuities.

For our particular problem we expect to obtain concentration profiles with steep gradients on the interface between the stratum corneum and the epidermis. This is a result of the discontinuity in the electric and diffusion parameters. Due to the very low conductivity, the stratum corneum acts like a barrier to the electric current, creating a steep gradient in the electric potential. This fact, associated to the very low diffusivity of this layer, results in a drug concentration profile with a sharp front at the interface between stratum corneum and epidermis.

To solve the advection dominated integro-differential equation (10) we use the method of lines approach: a spatial discretization followed by a time integration. In the spatial discretization we use an hybrid approach. It combines two distinct finite difference schemes, one suitable for the advective term and the other suitable for the diffusion like terms. The advective term is approximated by a high-order WENO scheme [21, 25] while the diffusion like terms are approximated by classical finite differences. This approach allows a straightforward and efficient time discretization by an IMEX multistep method. In the following we briefly outline this numerical procedure.

Let  $x_i$ ,  $i = 1, \dots, N$ , denote a uniform discretization of the spatial domain  $\Omega$ . We set  $x_{i+1} = x_i + \Delta x$ , with  $\Delta x$  the uniform mesh size,  $x_1 = -L_{dp}$ , and  $x_N = L_s$ . Let us also define  $x_{i+1/2} = x_i + \Delta x/2$ . It is important to remark that the nodes  $x_i$  coincide with the interface between the drug patch and the skin and also with the interfaces between the skin layers.

Let us rewrite (10) in the form

$$\frac{\partial c}{\partial t} = F(c) + G(c) \quad \text{in } \Omega \times (0, T]. \quad (32)$$

with

$$F(c) = \nabla \cdot f(c) \quad (33)$$

$f(c) = -vc$ , and

$$G(c) = \nabla \cdot (\tilde{D}_F \nabla c) + \int_0^t \nabla \cdot (e^{-(t-s)/\tau} \tilde{D}_{nF} \nabla c) ds. \quad (34)$$

We introduce in what follows the spatial discretization. As mentioned before, for the advection term we use a WENO discretization. The WENO schemes rely on convex combinations of well defined local stencils. Ideally, near discontinuities or sharp-gradients the weights are automatically adjusted such that the contributions from the smooth stencils are much more significant.

For a review on WENO methods we refer to [33]. We consider

$$F(c_i(t)) \approx \frac{f_{i+1/2}(t) - f_{i-1/2}(t)}{\Delta x} := F_h(c_i(t)). \quad (35)$$

where  $c_i(t) = c(x_i, t)$ ,  $f_{i\pm 1/2}(t)$  denotes an approximation for  $f(c(x_{i\pm 1/2}(t)))$ . In particular,  $f_{i+1/2}(t)$  is given by

$$f_{i+1/2}(t) = \omega_1 f_{i+1/2}^{(1)}(t) + \omega_2 f_{i+1/2}^{(2)}(t), \quad (36)$$

with  $f_{i+1/2}^{(1)}(t)$  and  $f_{i+1/2}^{(2)}(t)$  defined by the second-order approximations

$$f_{i+1/2}^{(1)}(t) = -\frac{1}{2}f(c_{i-1}(t)) + \frac{3}{2}f(c_i(t)) \quad \text{and} \quad f_{i+1/2}^{(2)}(t) = \frac{1}{2}f(c_i(t)) + \frac{1}{2}f(c_{i+1}(t)).$$

In (36),  $\omega_1$  and  $\omega_2$  are non-linear weights given by the formulas

$$\omega_m = \frac{\tilde{\omega}_m}{\tilde{\omega}_1 + \tilde{\omega}_2}, \quad \text{with} \quad \tilde{\omega}_m = \frac{\gamma_m}{(\epsilon + \beta_m)^2}, \quad m = 1, 2.$$

Here,  $\gamma_1 = 1/3$  and  $\gamma_2 = 2/3$  are usually called linear weights,  $\epsilon$  is a small positive constant to avoid zero division, and  $\beta_m$  are the so-called smoothness indicators defined by

$$\beta_1 = (f(c_i(t)) - f(c_{i-1}(t)))^2 \quad \text{and} \quad \beta_2 = (f(c_{i+1}(t)) - f(c_i(t)))^2.$$

This scheme is theoretically third-order accurate, at least in smooth regions [21, 25]. Note also that the approximation (36) is biased to the left respecting the upwind nature of the problem, i.e.,  $v \geq 0$ .

For the parabolic like term (34) the adopted semi-discrete finite difference discretization is defined by

$$G(c_i(t)) \simeq \nabla_h^*(\tilde{D}_F \nabla_h c_i(t)) + \int_0^t \nabla_h^*(e^{(-t+s)/\tau} \tilde{D}_{nF} \nabla_h c_i(s)) ds := G_h(c_i(t)),$$

where

$$\nabla_h^*(\tilde{D}_F \nabla_h c_i(t)) = \frac{1}{\Delta x^2} (\tilde{D}_{F,i+1/2}(c_{i+1}(t) - c_i(t)) - \tilde{D}_{F,i-1/2}(c_i(t) - c_{i-1}(t))),$$

being  $\nabla_h^*(e^{(-t+s)/\tau} \tilde{D}_{nF} \nabla_h c_i(s))$  defined analogously. This second order approximation in space is based on a standard second order centered finite difference operator. Since the finite differences nodes coincide with the several domain interfaces, possible discontinuities in the coefficients  $\tilde{D}_F$ ,  $\tilde{D}_{nF}$ , and  $\tau$  are well resolved by the proposed method. By  $c_h(t)$  we represent the semi-discrete approximation defined by the WENO scheme

$$c'_h(t) = F_h(c_h(t)) + G_h(c_h(t)), t \in (0, T], \quad (37)$$

The time integration is carried out by the second-order implicit-explicit backward differentiating formula (IMEX-BDF2). IMEX schemes are popular choices for problems of type (32). In particular, the IMEX-BDF2 is a two level method that has shown to present good stability properties when applied to advection-diffusion equations [20, 15]. Applying the IMEX-BDF2 to (37) we obtain the fully discrete scheme

$$c_h^{n+1} = \frac{4}{3}c_h^n - \frac{1}{3}c_h^{n-1} + \frac{\Delta t}{3} \left( 4F_h(c_h^n) - 2F_h(c_h^{n-1}) + 2G_h(c_h^{n+1}) \right), \quad (38)$$

with  $t_n = n\Delta t$ , where  $\Delta t$  the uniform time step,  $c_h^n$  denotes the numerical approximation for  $c(t_n)$ , and  $G_h(c_h^{n+1})$  is defined considering the rectangular rule in the integral term

$$\int_0^{t_{n+1}} \nabla_h^* \cdot (e^{-(t_{n+1}-t_j)/\tau} \tilde{D}_{nF} \nabla_h c_h(s)) ds \approx \Delta t \sum_{j=1}^{n+1} \nabla_h^* \cdot (e^{-(t_{n+1}-t_j)/\tau} \tilde{D}_{nF} \nabla_h c_h(t_j)).$$

The multistep method is initialized using a first order IMEX method consisting of the combination forward-backward Euler. To guarantee the stability of the method we have used the time step restriction

$$\Delta t \leq \beta \frac{\Delta x}{\max v_i},$$

with  $\beta$  equal to 0.5.

To avoid to store the solution at all time levels in the method (38) and to save computational time we exploit the fact that the kernel  $e^{-(t+s)/\tau}$  rapidly goes to zero when  $s$  moves from  $t$ . In practice the method (38) is coupled with the truncation of the quadrature summation when the relative maximum change is below a predefined threshold (set to 1e-5 in our experiments). The numerical solution is stored in a dynamic matrix. The size of this matrix is continuously adjusted to  $N_x \times N_q$ , where  $N_x$  is the fixed size of the spatial mesh and  $N_q$  is given by  $N_q = N_n + N_n/2$ , or  $N_q = n$  if  $N_n + N_n/2 > n$ , with  $N_n$  the number of iterations needed to truncate the summation at the time iteration  $n$ . The performance of the proposed numerical scheme is illustrated in the appendix Numerical validation.

## 5. Numerical simulation

We start this section by discussing the parameters of the model. In what concerns skin viscoelastic properties several experimental studies with somewhat different results are reported in the literature. Here, we use the experimental data available in [6]. This is a detailed study where the mechanical properties for each of the three skin layers (stratum corneum, viable epidermis, and dermis) are individually quantified. Regarding conductivity, drug diffusivity, and thickness in a young skin, we used the values reported in [3], [3, 30, 31], and [3, 19, 24, 30], respectively. The values used in the simulations are summarized in Table 1. The drug gel (Polyacrylamide gels, 20% acrylamide) viscoelastic parameters were obtained from [16] and are also given in Table 1.

	Drug gel	Stratum corneum	Viable epidermis	Dermis	References
Thickness (cm)	1e-2	2e-3	4e-3	0.1	[3, 24, 19, 30]
$\psi_i$ ( $1/\Omega m$ )	1.5	1e-5	1e-2	1.5e-2	[3]
$D_{i,F}$ ( $m^2/s$ )	1e-8	1e-14	1e-11	3e-11	[3, 30, 31]
$D_{i,v}$ ( $g/(s m MPa)$ )	1e-9	1e-15	1e-12	3e-12	fixed
$E_{0,i}$ (MPa)	0.35	0.34	0.13	4.21	[6, 16]
$E_{1,i}$ (MPa)	0.07	0.23	0.25	2.16	[6, 16]
$\mu_i$ (MPa s)	0.26	0.33	0.65	6.17	[6, 16]

TABLE 1. Parameters used in the simulation (Young skin).

Now we address the relation between aging and skin properties. The Young's modulus of the skin increases with age, particularly in the stratum corneum and the viable epidermis [7, 19, 24, 32]. According to [32] the relaxation time also increases with age. The relation between skin thickness and aging is not completely clear. Many studies report that skin thickness decreases with age but reports of unchanged or even increased thickness are also available. It has been suggested that these variations are associated with sun exposition. Namely, skin thickness decreases with age in sun protected skin and increases with age in sun exposed skin. It has been also reported that the thickness of the stratum corneum does not change with age in sun protected skin [7, 24, 37]. A decrease in conductivity with increasing age is mentioned in [26, 27]. Based on these observations, and assuming a decrease in skin thickness, we report in Table 2 the parameters adopted for an aged skin. There are still two parameters arising in the definition of the Fickian and non-Fickian diffusion coefficients (7), namely,  $\alpha_i$  and  $D_{i,v}$ , that need to

be fixed. Here, to simplify we assume that  $\alpha_i = 1$  ( $\text{m}^3/\text{g}$ ) and  $D_{i,v} = K_i D_{i,F}$  with  $K_i = \frac{1}{10}$  ( $\text{g}/(\text{m}^3\text{MPa})$ )

	Drug gel	Stratum corneum	Viable epidermis	Dermis	References
Thickness (cm)	1e-2	2e-3	2.4e-3	0.06	[7, 24, 37]
$\psi_i$ ( $1/\Omega m$ )	1.5	9e-6	9e-3	1.35e-2	[26, 27]
$D_{i,F}$ ( $\text{m}^2/\text{s}$ )	1e-8	1e-14	1e-11	3e-11	[3, 30, 31]
$D_{i,v}$ ( $\text{g}/(\text{s m MPa})$ )	1e-9	1e-15	1e-12	3e-12	fixed
$E_{0,i}$ (MPa)	0.35	0.44	0.17	5.47	[7, 19, 24, 32]
$E_{1,i}$ (MPa)	0.07	0.30	0.33	2.81	[7, 19, 24, 32]
$\mu_i$ (MPas)	0.26	0.36	0.72	6.79	[32]

TABLE 2. Parameters used in the simulation (aging skin with decreased thickness of viable epidermis and dermis but same stratum corneum depth).

Numerical experiments are given next. For an aged skin we consider two scenarios: decreased thickness (according to the parameters given in Table 2) and unchanged thickness. The influence of the viscoelastic parameters is also addressed. For the simulations we have used  $\Delta x = 1e - 6$ .

*The potential and the Fickian and non-Fickian behaviours*

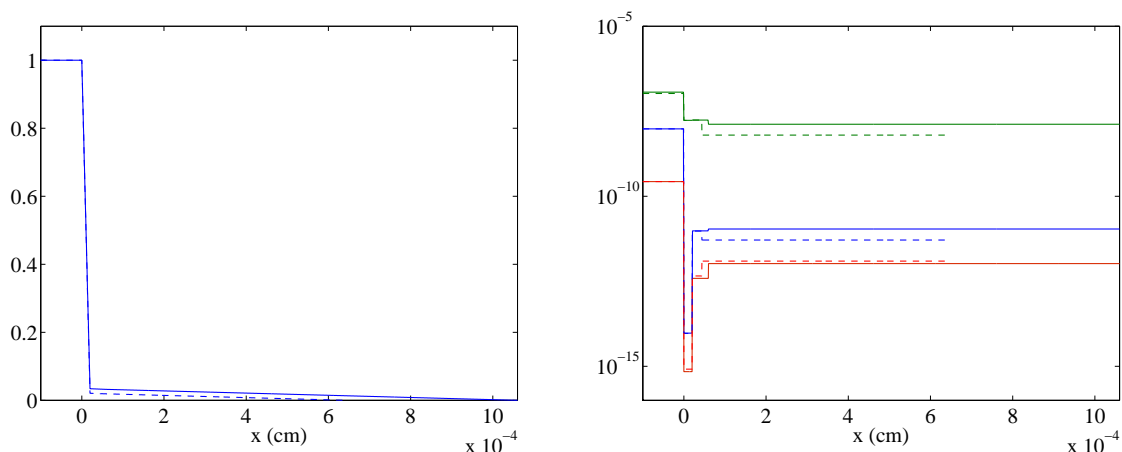


FIGURE 1. From left to right: voltage  $\phi$  with  $\phi(0) = 1$  and corresponding velocity  $v$  (in green), diffusion coefficient  $\tilde{D}_{i,F}$  (in blue), and the viscoelastic diffusion coefficient  $\tilde{D}_{i,nF}$  (in red). The results for young skin are represented with solid lines while the results for aged skin are represented with dashed lines.

A typical voltage  $\phi$  profile for a young skin and an aged skin is exhibited in Figure 1 (left) where the results for young skin are represented with solid lines and the results for an aged skin are represented with dashed lines. In Figure 1 (right) a plot of the corresponding velocity  $v$  is showed. The representation of diffusion coefficients  $\tilde{D}_{i,F}$  and  $\tilde{D}_{i,nF}$  is also exhibited. Figure 1 illustrates the convection-dominated character of the problem. We note the steep voltage gradient at the stratum corneum and the difference in magnitude between velocity and diffusion.

### *Absorption in young and aging skins*

In Figures 2 and 3 we compare the time evolution of drug profiles for young and aging skins characterized by the parameters in Tables 1 and 2 respectively. In Figure 2 (left) the mass of drug in %,  $\frac{M(t)}{M(0)}$ , in an young skin at instant  $t$  is plotted (red line). The total mass of drug absorbed by the capillary bed,  $M_{ab}(t) = \frac{1}{M(0)}(M(0) - M(t))$ , is represented in green. In Figure 2 (right) the mass of drug in an aging skin at time  $t$  is plotted in red while  $M_{ab}(t)$  is plotted in green. The plots in blue represent the evolution of drug in the reservoir. In both cases a constant voltage of  $1V$  was applied for  $360\text{ min}$ . The dashed vertical line indicates the time when the voltage is turned off. As it can be seen, the evolution of the drug profile in the reservoir is identical in both cases. In Figure 3, the time profiles for the drug

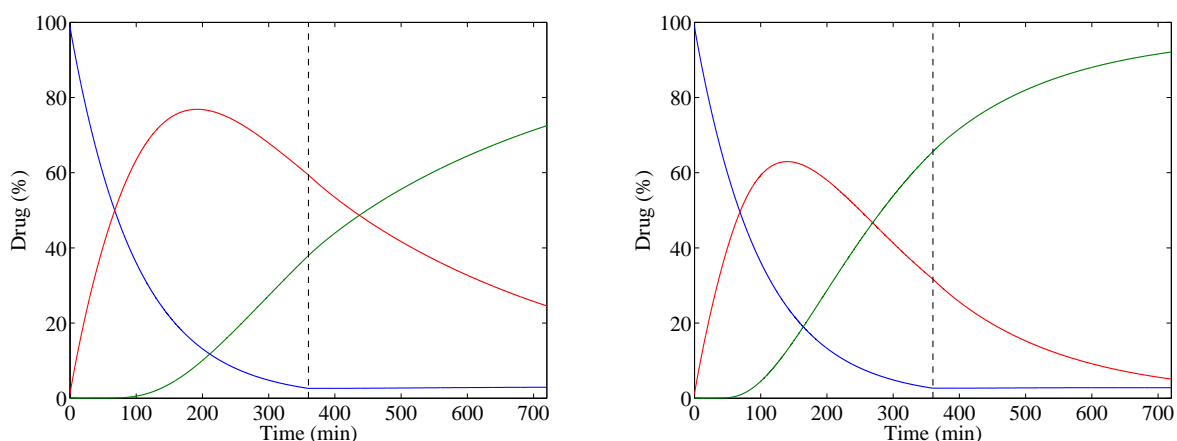


FIGURE 2. From left to right: young skin and aging skin. Percentage of the drug in the reservoir (blue line), in the skin (red line), and percentage of drug absorbed (green line).

percentage in the skin,  $M_s(t) = \frac{1}{M(0)}(M(t) - M_{dp}(t))$ , where  $M_{dp}(t)$  denotes the drug mass in the reservoir, as well as for the drug absorbed,  $M_{ab}(t)$  are compared. We observe that for the same electrical protocol the percentage of drug absorbed after 720 min was around 70% in the young skin and around 90% in the aged skin. These findings suggest that for the data contained in Tables 1 and 2, drug absorption in an aging skin, with larger Young modulus and smaller thickness, is much faster than in a young skin.

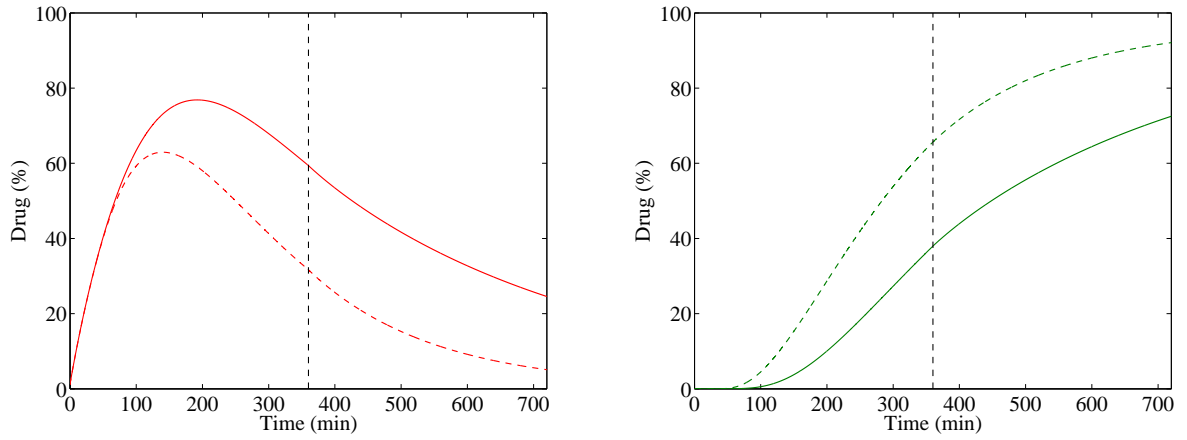


FIGURE 3. From left to right: percentage of drug in the skin  $M_s(t)$  and percentage of total drug absorbed  $\frac{M_{ab}(t)}{M(0)}$ . Young skin (solid line) and aging skin (dashed line). The young skin is characterized by the parameters in Table 1. The aging skin is characterized by the parameters in Table 2.

### *Tuning the applied voltage*

A relevant question is how we can tune the electrical field in order to slow down the delivery in the capillary bed, in the case of an aging skin. As shown in Figure 4 this can be achieved applying 0.3V for 360min in the aging skin.

### *Absorption in young and aging skins: viscoelastic effects*

In Figures 3 and 4 we illustrate the effect of two combined characteristics of an aging skin: loss of elasticity and thinning. We now study separately the two effects. In Figure 5, we illustrate the influence of viscoelasticity in an aging skin. For that, we repeat the previous example (1V for 360 min) considering now that the aging skin is characterized by the parameters in

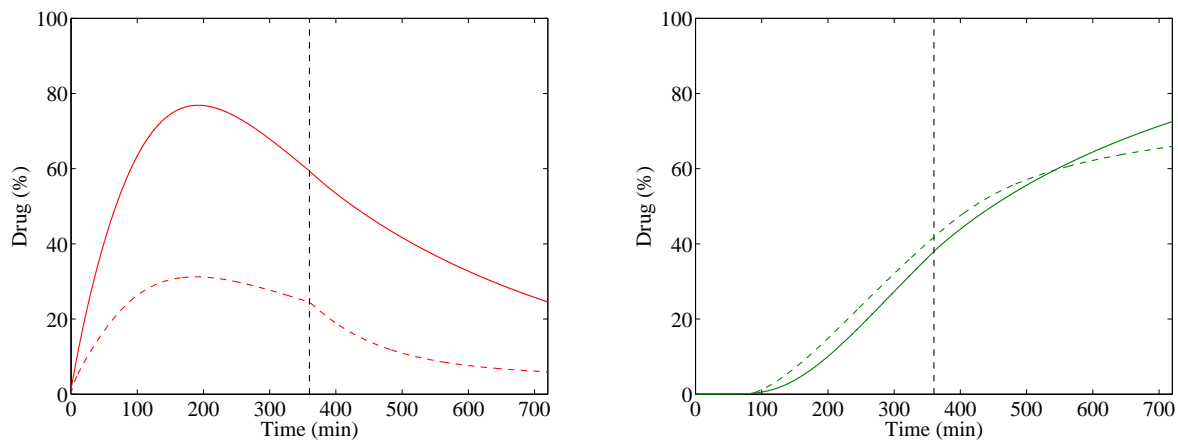


FIGURE 4. From left to right: percentage of drug in the skin,  $M_s(t)$ , and percentage of drug absorbed  $\frac{M_{ab}(t)}{M(0)}$ . Young skin (solid line) and aged skin (dashed line). Electric protocol:  $0.3V$  (aged skin) and  $1V$  (young skin) applied for  $360 \text{ min}$ .

Table 3. This means that we assume that aging only implies thinning, and that the viscoelastic properties of the aging skin are the same as for a young skin (Table 1).

	Drug gel	Stratum corneum	Viable epidermis	Dermis
Thickness (cm)	1e-2	2e-3	2.4e-3	0.06
$\psi_i$ ( $1/\Omega m$ )	1.5	9e-6	9e-3	1.35e-2
$D_{i,F}$ ( $m^2/s$ )	1e-8	1e-14	1e-11	3e-11
$D_{i,v}$ ( $g/(s m MPa)$ )	1e-9	1e-15	1e-12	3e-12
$E_{0,i}$ (MPa)	0.35	0.34	0.13	4.21
$E_{1,i}$ (MPa)	0.07	0.23	0.25	2.16
$\mu_i$ (MPa s)	0.26	0.33	0.65	6.17

TABLE 3. Parameters used in the simulation of an aging skin (Table 2) with the Young modulus of a young skin (Table 1).

As shown in Figure 5, the impact of these parameters is noticeable. We observe that if we adopt the characterization of aging skin as defined in Table 3, then the percentage of absorbed drug increases significantly. In fact with the parameters in Table 3, the opposition to the permeation of drug is relaxed, relatively to the parameters in Table 2. These results indicate that mathematical models for transdermal drug absorption should take into account the loss of elasticity induced by aging.

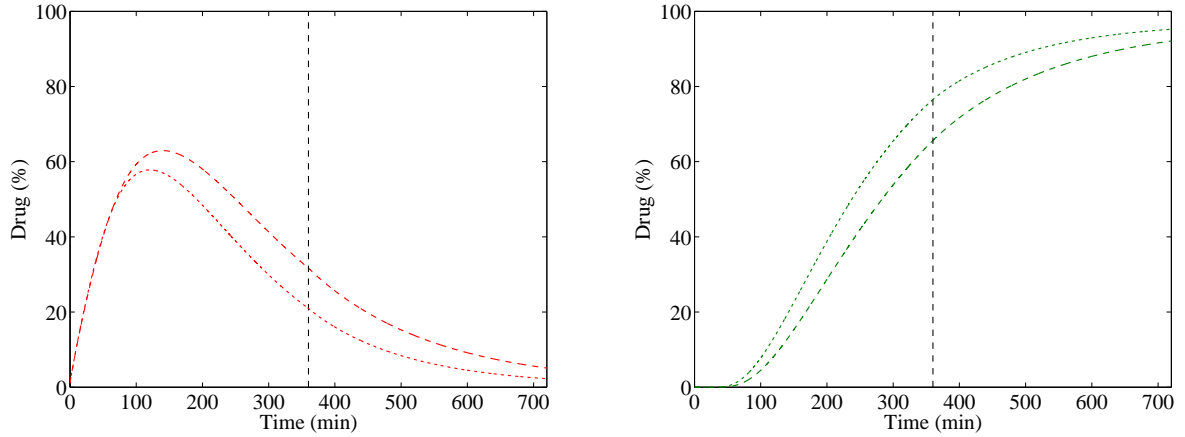


FIGURE 5. From left to right: Percentage of drug mass  $M_s(t)$  and percentage of drug absorbed  $\frac{M_{ab}(t)}{M(0)}$  in an aging skin: with the parameters of Table 2 (dash line) and with the parameters of Table 3 (dot line).

Finally, for illustration purposes, we show in Figure 6, spatial drug concentration profiles for an aging skin at four different times.

#### *Aging skin: the thickness effect*

There is a controversy in the medical literature regarding the effect of aging in drug percutaneous penetration [23]. The controversy occurs because skin aging is characterized by the simultaneous loss of elasticity and thinning. The two phenomena produce opposite effects: the lost of elasticity, described by the increase in Young modulus and viscosity, slows absorption. On the contrary, thinning of skin layers speeds up absorption by the capillary bed.

In Figures 2 and 3 we observe that if we take into account the stiffness and thickness alterations induced by aging in the skin, then drug is absorbed by a young skin with a slower rate. This slowing down is confirmed in Figure 5, where only alterations of Young modulus are considered.

In what follows we show that if the thickness reduction is not taken into account then the reverse is observed. We consider for the aging skin the parameters given in Table 2, but we assume that the thickness is the same as the one of the young skin (Table 1).

In Figures 7, we compare the time evolution of drug profiles for young and aging skins. A constant voltage of  $1V$  was applied for  $360\text{ min}$ . We observe that now the percentage of drug absorbed after  $720\text{ min}$  is higher in the young

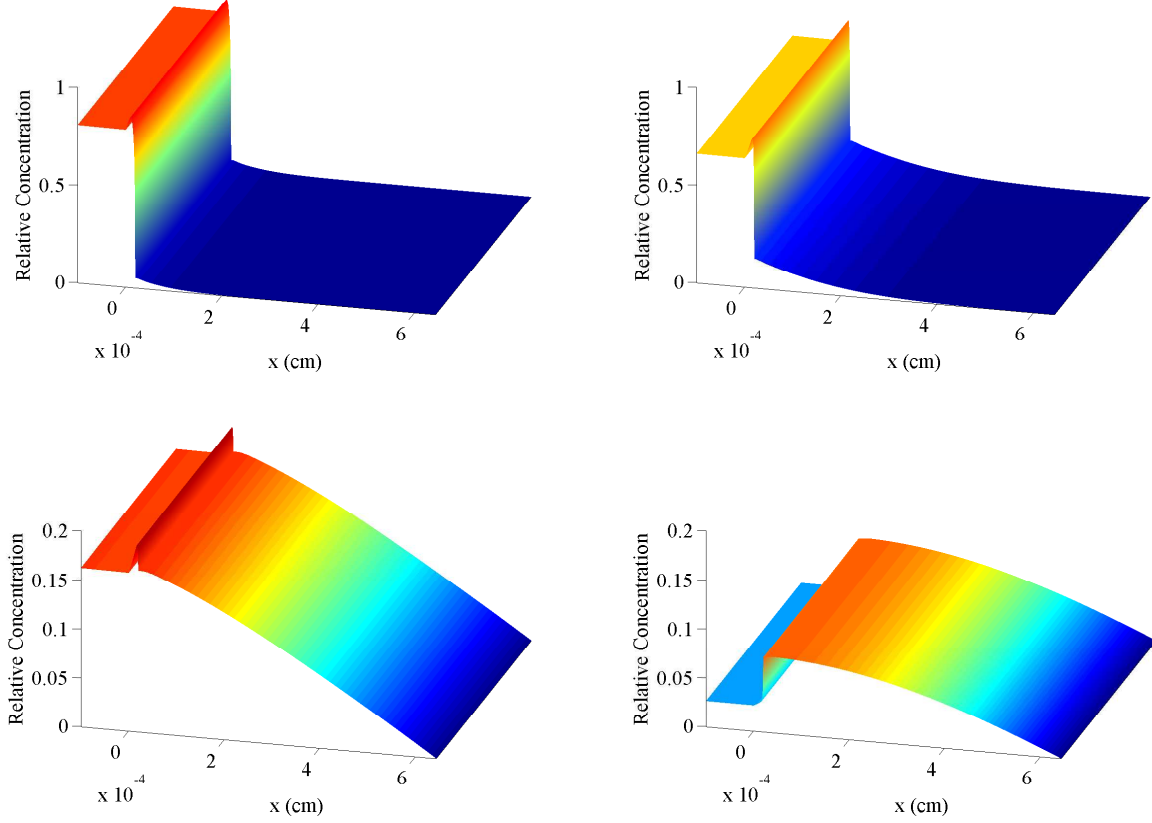


FIGURE 6. From left to right and top to bottom: drug concentration in an aging skin at  $t = 20, 40, 180, 360(\text{min})$ , respectively. In the simulation the parameters of Table 2 were considered and an electric protocol of  $1V$  for  $360 \text{ min}$ .

	Drug gel	Stratum corneum	Viable epidermis	Dermis
Thickness (cm)	1e-2	2e-3	4e-3	0.1
$\psi_i$ ( $1/\Omega m$ )	1.5	9e-6	9e-3	1.35e-2
$D_{i,F}$ ( $m^2/s$ )	1e-8	1e-14	1e-11	3e-11
$D_{i,v}$ ( $g/(s m MPa)$ )	1e-9	1e-15	1e-12	3e-12
$E_{0,i}$ (MPa)	0.35	0.44	0.17	5.47
$E_{1,i}$ (MPa)	0.07	0.30	0.33	2.81
$\mu_i$ (MPa.s)	0.26	0.36	0.72	6.79

TABLE 4. Parameters used in the simulation of an aging skin (Table 2) with the thickness of a young skin (Table 1).

skin than in the aging skin. The difference is around 15%. These findings

suggest that drug absorption in an aging skin with unchanged thickness is slower than in a young skin.

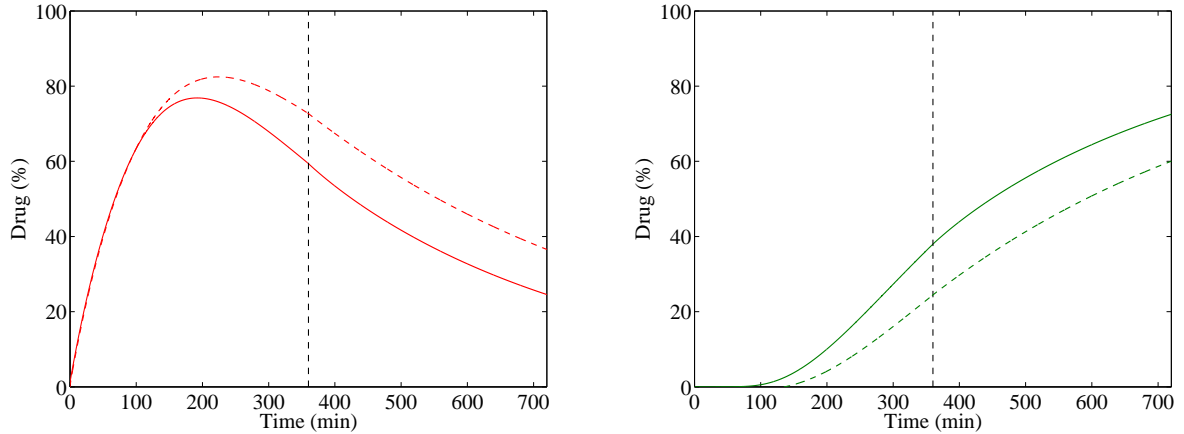


FIGURE 7. From left to right: mass of drug (%) in the skin,  $M_s(t)$ , and percentage of drug absorbed  $\frac{M_{ab}(t)}{M(0)}$ . Young skin (solid line) and aged skin (dashed line). It is assumed that the skin thickness does not change with age.

## 6. Conclusions: Are laboratorial experiments wrong?

In this paper the multilayer viscoelastic initial boundary value problem (10), (11), (12), (13), and (22) with the velocities  $\bar{v}_i, i = dp, sc, e, d$ , defined by the boundary value problem (15), (16), (17) and (18), for iontophoretic transdermal drug delivery was proposed and analyzed. The coupled system consists of integro-differential equations, for drug transport, that take into account the viscoelastic nature of the skin layers and an elliptic equation for the electric potential.

The paper contains original contributions from a mathematical point of view-analytical and numerical-and also regarding the medical outcomes. From the mathematical point of view we derived analytical estimates for  $M(t)$  and  $M_{ab}(t)$ , (28), (29), respectively, where the upper and lower bounds have a sound physical meaning. Consequently, these estimates, besides being an analytical tool to study stability, also exhibit an instrumental value. Namely we prove that:

- (a) the upper bound for the mass of drug in the reservoir-skin system is a decreasing function of the skin's Young modulus and of the thicknesses of the skin layers;
- (b) the lower bound for the mass of drug absorbed by the capillary bed is an increasing function of the skin's Young modulus and of the thicknesses of the skin layers.

From the numerical point of view an efficient numerical scheme was proposed - the multistep method (38) coupled with the truncation strategy for the integral approximation introduced in Section 4. Numerical experiments illustrating the accuracy and the efficiency of the numerical method and the behavior of the mathematical model are presented.

Regarding the medical outcomes the ultimate aim of the paper is to clarify the ongoing controversy, in the medical literature, concerning the absorption of drug in an aging skin. This controversy is illustrated by the opposite answers that can be found, to questions like "Does age matters?" or "Is absorption slowed down or speeded up in an aging skin?" ([4, 7, 8, 19, 22, 23, 24, 32, 34, 36, 37]).

The model proposed in this paper shows that opposite answers are given to such questions, because the aging skin is not accurately characterized. In fact the two main alterations that can occur in an aging skin must be analyzed separately:

- (i) A loss of elasticity: aging induces degeneration in the elastin and collagen fibers, particularly in the stratum corneum and in the viable epidermis, that leads to an increase in the Young's modulus [7, 19, 24, 32].
- (ii) A thinning of skin layers, due to aging, genetics or medications.

We note that (i) and (ii) produce opposite effects. Larger Young modulus and viscosities represent a hindrance to drug absorption by the capillary bed; on the contrary, thinning acts as an enhancement, because molecules must travel shorter distances to penetrate the blood system. "Is absorption slowed down or speeded up in an aging skin?" The balance of these two aging factors - stiffness and thickness - dictates the fate of drug absorption. In fact, both situations are admissible and the apparent controversy is due to a lack of clarity in the characterization of the aging patients participating in the medical experiments. To circumvent the problem, the two main alterations of an aging skin - stiffness and thickness - must be taken into account. If in a

certain patient the increase of stiffness dominates the decrease of thickness, then absorption is slowed down (Figure 7); on the contrary if the skin's thinning dominates the increase of stiffness, the absorption is speeded up (Figures 2, 3 and 5). To conclude, we observe that due to the differences between young and aging skin, the electrical protocols should be tuned in accordance to the characteristics of the aging patient's skin (Figure 4).

## 7. Appendix - Stability

**Proof of Proposition 1:** From (23), to get an upper bound for

$$\sum_{i=dp,sc,e,d} \|c_i(t)\|_{L^2(\Omega_i)}^2 + \sum_{i=dp,sc,e,d} \tilde{D}_{i,nF} \int_0^t \|e^{-\frac{t-s}{\tau_i}} \nabla c_i(s)\|_{L^2(\Omega_i)}^2 ds,$$

we need to get estimates for  $(J_i(t), \nabla c_i(t))_{L^2(\Omega_i)}$  for  $i = dp, sc, e, d$ . To obtain an upper bound for  $(J_{i,io}(t), \nabla c_i(t))_{L^2(\Omega_i)}$  we start by remarking that if  $c(t) \in H_0^1(\Omega)$  denotes the drug concentration in  $\Omega$ , then there exists a positive constant  $C_P$  such that

$$\begin{aligned} \left( \sum_{i=dp,sc,e,d} \|c_i(t)\|_{L^2(\Omega_i)}^2 \right)^{1/2} &= \|c(t)\|_{L^2(\Omega)} \\ &\leq C_P \|\nabla c(t)\|_{L^2(\Omega)} \\ &= C_P \left( \sum_{i=dp,sc,e,d} \|\nabla c_i(t)\|_{L^2(\Omega_i)}^2 \right)^{1/2}. \end{aligned}$$

Consequently, we have

$$\begin{aligned} \sum_{i=dp,sc,e,d} |(J_{i,io}(t), \nabla c_i(t))_{L^2(\Omega_i)}| &\leq \sum_{i=dp,sc,e,d} \|\bar{v}_i\|_{L^\infty(\Omega_i)} \|c_i(t)\|_{L^2(\Omega_i)} \|\nabla c_i(t)\|_{L^2(\Omega_i)} \\ &\leq \left( \sum_{i=dp,sc,e,d} \|c_i(t)\|_{L^2(\Omega_i)}^2 \right)^{1/2} \left( \sum_{i=dp,sc,e,d} \|\bar{v}_i\|_{L^\infty(\Omega_i)}^2 \|\nabla c_i(t)\|_{L^2(\Omega_i)}^2 \right)^{1/2} \\ &\leq C_P \left( \sum_{i=dp,sc,e,d} \|\nabla c_i(t)\|_{L^2(\Omega_i)}^2 \right)^{1/2} \left( \sum_{i=dp,sc,e,d} \|\bar{v}_i\|_{L^\infty(\Omega_i)}^2 \|\nabla c_i(t)\|_{L^2(\Omega_i)}^2 \right)^{1/2} \\ &\leq C_P \max_{i=dp,sc,e,d} \|\bar{v}_i\|_{L^\infty(\Omega_i)} \sum_{i=dp,sc,e,d} \|\nabla c_i(t)\|_{L^2(\Omega_i)}^2. \end{aligned} \tag{39}$$

We consider now  $(J_{i,F}(t) + J_{i,nF}(t), \nabla c_i(t))_{L^2(\Omega_i)}$ . We have

$$\begin{aligned} -(J_{i,F}(t) + J_{i,nF}(t), \nabla c_i(t))_{L^2(\Omega_i)} &= \tilde{D}_{iF} \|\nabla c_i(t)\|_{L^2(\Omega_i)}^2 \\ &\quad - \tilde{D}_{i,nF} \int_0^t e^{-\frac{t-s}{\tau_i}} (\nabla c_i(s), \nabla c_i(t)) ds. \end{aligned} \quad (40)$$

Then from (23) we obtain

$$\begin{aligned} &\frac{1}{2} \sum_{i=dp,sc,e,d} \frac{d}{dt} \|c_i(t)\|_{L^2(\Omega_i)}^2 \\ &\quad + \left( \min_{i=dp,sc,e,d} \tilde{D}_{iF} - C_P \max_{i=dp,sc,e,d} \|\bar{v}_i\|_{L^\infty(\Omega_i)} \right) \sum_{i=dp,sc,e,d} \|\nabla c_i(t)\|_{L^2(\Omega_i)}^2 \\ &\quad + \sum_{i=dp,sc,e,d} \tilde{D}_{i,nF} \int_0^t e^{-\frac{t-s}{\tau_i}} (\nabla c_i(s), \nabla c_i(t)) ds \leq 0. \end{aligned} \quad (41)$$

We observe now that

$$\begin{aligned} \tilde{D}_{i,nF} \int_0^t e^{-\frac{t-s}{\tau_i}} (\nabla c_i(s), \nabla c_i(t)) ds &= \frac{1}{2} \frac{d}{dt} \tilde{D}_{i,nF} \left\| \int_0^t e^{-\frac{t-s}{\tau_i}} \nabla c_i(s) ds \right\|_{L^2(\Omega_i)}^2 \\ &\quad + \frac{1}{\tau_i} \tilde{D}_{i,nF} \left\| \int_0^t e^{-\frac{t-s}{\tau_i}} \nabla c_i(s) ds \right\|_{L^2(\Omega_i)}^2. \end{aligned} \quad (42)$$

The last representation leads to

$$\begin{aligned} &\frac{1}{2} \sum_{i=dp,sc,e,d} \frac{d}{dt} \|c_i(t)\|_{L^2(\Omega_i)}^2 \\ &\quad + \left( \min_{i=dp,sc,e,d} \tilde{D}_{iF} - C_P \max_{i=dp,sc,e,d} \|\bar{v}_i\|_{L^\infty(\Omega_i)} \right) \sum_{i=dp,sc,e,d} \|\nabla c_i(t)\|_{L^2(\Omega_i)}^2 \\ &\quad + \frac{1}{2} \sum_{i=dp,sc,e,d} \frac{d}{dt} \tilde{D}_{i,nF} \left\| \int_0^t e^{-\frac{t-s}{\tau_i}} \nabla c_i(s) ds \right\|_{L^2(\Omega_i)}^2 \\ &\quad \leq - \sum_{i=dp,sc,e,d} \frac{1}{\tau_i} \tilde{D}_{i,nF} \left\| \int_0^t e^{-\frac{t-s}{\tau_i}} \nabla c_i(s) ds \right\|_{L^2(\Omega_i)}^2. \end{aligned} \quad (43)$$

Considering now the assumption (24) we get from (43)

$$\begin{aligned}
& \sum_{i=dp,sc,e,d} \frac{d}{dt} \|c_i(t)\|_{L^2(\Omega_i)}^2 + \sum_{i=dp,sc,e,d} \frac{d}{dt} \tilde{D}_{i,nF} \left\| \int_0^t e^{-\frac{t-s}{\tau_i}} \nabla c_i(s) ds \right\|_{L^2(\Omega_i)}^2 \\
& \leq - \sum_{i=dp,sc,e,d} \frac{2}{\tau_i} \tilde{D}_{i,nF} \left\| \int_0^t e^{-\frac{t-s}{\tau_i}} \nabla c_i(s) ds \right\|_{L^2(\Omega_i)}^2 \\
& \quad - \frac{2}{C_P^2} \left( \min_{i=dp,sc,e,d} \tilde{D}_{iF} - C_P \max_{i=dp,sc,e,d} \|\bar{v}_i\|_{L^\infty(\Omega_i)} \right) \sum_{i=dp,sc,e,d} \|c_i(t)\|_{L^2(\Omega_i)}^2 \\
& \leq \max \left\{ - \min_{i=dp,sc,e,d} \frac{2}{\tau_i}, - \frac{2}{C_P^2} \left( \min_{i=dp,sc,e,d} \tilde{D}_{iF} - C_P \max_{i=dp,sc,e,d} \|\bar{v}_i\|_{L^\infty(\Omega_i)} \right) \right\} \\
& \quad \left( \sum_{i=dp,sc,e,d} \|c_i(t)\|_{L^2(\Omega_i)}^2 + \sum_{i=dp,sc,e,d} \tilde{D}_{i,nF} \left\| \int_0^t e^{-\frac{t-s}{\tau_i}} \nabla c_i(s) ds \right\|_{L^2(\Omega_i)}^2 \right). \tag{44}
\end{aligned}$$

An estimate for  $\sum_{i=dp,sc,e,d} \|c_i(t)\|_{L^2(\Omega_i)}^2 + \sum_{i=dp,sc,e,d} \tilde{D}_{i,nF} \int_0^t \|e^{-\frac{t-s}{\tau_i}} \nabla c_i(s)\|_{L^2(\Omega_i)}^2 ds$  is easily obtained now from (44). As  $c \in C^1([0, T], L^2(\Omega))$  we conclude (25).  $\blacksquare$

**Proof of Proposition 3:** We start by remarking that instead of (23) we have

$$\begin{aligned}
\frac{1}{2} \sum_{i=dp,sc,e,d} \frac{d}{dt} \|c_i(t)\|_{L^2(\Omega_i)}^2 - \sum_{i=dp,sc,e,d} (J_i(t), \nabla c_i(t))_{L^2(\Omega_i)} \\
+ \beta_{dp,sc} (c_{dp}(0, t) - c_{sc}(0, t))^2 = 0. \tag{45}
\end{aligned}$$

As

$$|(J_{i,io}(t), \nabla c_i(t))_{L^2(\Omega_i)}| \leq \frac{1}{4\epsilon_{i,1}^2} \|c_i(t)\|_{L^2(\Omega_i)}^2 + \epsilon_{i,1}^2 \|\bar{v}_i\|_{L^\infty(\Omega_i)}^2 \|\nabla c_i(t)\|_{L^2(\Omega_i)}^2,$$

where  $\epsilon_{i,1} \neq 0$  are arbitrary constants,  $i = dp, sc, e, d$ , and (40), (42) hold, from (45) we get

$$\begin{aligned}
& \sum_{i=dp,sc,e,d} \frac{d}{dt} \|c_i(t)\|_{L^2(\Omega_i)}^2 + \sum_{i=dp,sc,e,d} 2 \left( \tilde{D}_{iF} - \epsilon_{i,1}^2 \|\bar{v}_i\|_{L^\infty(\Omega_i)}^2 \right) \|\nabla c_i(t)\|_{L^2(\Omega_i)}^2 \\
& \quad + \sum_{i=dp,sc,e,d} \frac{d}{dt} \tilde{D}_{i,nF} \left\| \int_0^t e^{-\frac{t-s}{\tau_i}} \nabla c_i(s) ds \right\|_{L^2(\Omega_i)}^2 \\
& \leq \sum_{i=dp,sc,e,d} \frac{1}{2\epsilon_{i,1}^2} \|c_i(t)\|_{L^2(\Omega_i)}^2 - \sum_{i=dp,sc,e,d} \frac{2}{\tau_i} \tilde{D}_{i,nF} \left\| \int_0^t e^{-\frac{t-s}{\tau_i}} \nabla c_i(s) ds \right\|_{L^2(\Omega_i)}^2 \\
& \quad - 2\beta_{dp,sc} (c_{dp}(0, t) - c_{sc}(0, t))^2.
\end{aligned} \tag{46}$$

Fixing now, in (46),  $\epsilon_{i,1}^2 = \frac{\tilde{D}_{iF}}{2\|\bar{v}_i\|_{L^\infty(\Omega_i)}^2}$ ,  $dp, sc, e, d$ , we obtain

$$\begin{aligned}
& \frac{d}{dt} \left( \sum_{i=dp,sc,e,d} \|c_i(t)\|_{L^2(\Omega_i)}^2 + \sum_{i=dp,sc,e,d} \tilde{D}_{iF} \|\nabla c_i(t)\|_{L^2(\Omega_i)}^2 \right. \\
& \quad \left. + \sum_{i=dp,sc,e,d} \tilde{D}_{i,nF} \left\| \int_0^t e^{-\frac{t-s}{\tau_i}} \nabla c_i(s) ds \right\|_{L^2(\Omega_i)}^2 \right) \\
& \leq \sum_{i=dp,sc,e,d} \frac{\|\bar{v}_i\|_{L^\infty(\Omega_i)}^2}{\tilde{D}_{iF}} \|c_i(t)\|_{L^2(\Omega_i)}^2 - \sum_{i=dp,sc,e,d} \frac{2}{\tau_i} \tilde{D}_{i,nF} \left\| \int_0^t e^{-\frac{t-s}{\tau_i}} \nabla c_i(s) ds \right\|_{L^2(\Omega_i)}^2 \\
& \quad - 2\beta_{dp,sc} (c_{dp}(0, t) - c_{sc}(0, t))^2,
\end{aligned} \tag{47}$$

that allows us the establishment of the following inequality

$$\begin{aligned}
& \sum_{i=dp,sc,e,d} \|c_i(t)\|_{L^2(\Omega_i)}^2 + \sum_{i=dp,sc,e,d} \tilde{D}_{iF} \|\nabla c_i(t)\|_{L^2(\Omega_i)}^2 \\
& \quad + \sum_{i=dp,sc,e,d} \tilde{D}_{i,nF} \left\| \int_0^t e^{-\frac{t-s}{\tau_i}} \nabla c_i(s) ds \right\|_{L^2(\Omega_i)}^2 \\
& \leq \max_{i=dp,sc,e,d} \frac{\|\bar{v}_i\|_{L^\infty(\Omega_i)}^2}{\tilde{D}_{iF}} \left( \sum_{i=dp,sc,e,d} \int_0^t \|c_i(s)\|_{L^2(\Omega_i)}^2 ds \right. \\
& \quad \left. + \sum_{i=dp,sc,e,d} \tilde{D}_{i,nF} \int_0^t \left\| \int_0^s e^{-\frac{s-\mu}{\tau_i}} \nabla c_i(\mu) d\mu \right\|_{L^2(\Omega_i)}^2 ds \right) \\
& \quad + \|c_{dp}(0)\|_{L^2(\Omega_{dp})}^2 - 2\beta_{dp,sc} \int_0^t (c_{dp}(0, s) - c_{sc}(0, s))^2 ds,
\end{aligned} \tag{48}$$

for  $t \in [0, T]$ . Finally, the application of the Gronwall's lemma leads to (31). ■

## 8. Appendix - Numerical validation

To illustrate the proposed numerical scheme we solve two problems, one with smooth coefficients and known exact solution (Example 1) and the other with discontinuous coefficients and unknown exact solution (Example 2). In both problems we set a homogeneous Neumann boundary condition at the left boundary and a homogeneous Dirichlet boundary condition at the right boundary. To handle the boundary conditions we consider extra points whenever required. Then, at the Neumann boundary, we use finite difference approximations to estimate the solution at these extra points. At the Dirichlet boundary we set the solution at the extra points equal to zero.

**Example 1.** *In this example we consider  $\Omega = [0, 1]$ , and we define the initial condition and a source term  $f$ , such that, the exact solution is given by*

$$c(x, t) = e^t \cos(2\pi x)(1 - x^2).$$

*We also set the coefficients  $v = 1$ ,  $\tilde{D}_F = 1$ ,  $\tau = 1$ , and  $\tilde{D}_{nF} = 1$ . The simulation time is  $T = 2$ . To test the accuracy of the numerical scheme we successively halve the mesh size, from  $\Delta x = 0.02$  to  $\Delta x = 0.005$ , and measure the numerical error using the  $L_\infty$ -norm. The results are given in Figure 8 and they illustrate the expected second-order convergence rate.*

**Example 2.** *In this example we consider  $\Omega = [0, 1]$ , the initial condition*

$$c_0 = e^{-(x-0.25)^2/0.002}$$

*and the coefficients*

$$v = \begin{cases} 1e-3, & x \leq 0.5 \\ 2e-3, & x > 0.5 \end{cases} \quad \tilde{D}_F = \begin{cases} 1e-6, & x \leq 0.5 \\ 1e-7, & x > 0.5 \end{cases}$$

$$\tau = \begin{cases} 1, & x \leq 0.5 \\ 2, & x > 0.5 \end{cases} \quad \tilde{D}_{nF} = \begin{cases} 1e-7, & x \leq 0.5 \\ 1e-5, & x > 0.5 \end{cases}$$

*In Figure 9 we present the numerical solution obtained with the proposed scheme for  $\Delta x = 0.002$  and at time equal 0, time equal 4, and time equal 7. The results show that the boundary layer arising at the discontinuity*

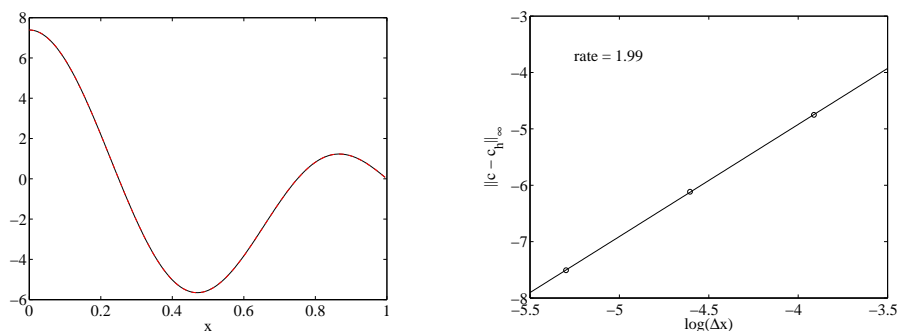


FIGURE 8. At the left: exact solution (solid black line) and numerical solution (dashed red line) at time equal 2 and  $\Delta x = 0.005$  for Example 1. At the right: estimated convergence rate in the  $L_\infty$ -norm, where the error  $\|c - c_h\|_\infty$  is the maximum over all time levels of  $\|c(t_n) - c_h^n\|_\infty$ .

*point is well resolved with no signs of numerical instabilities.*

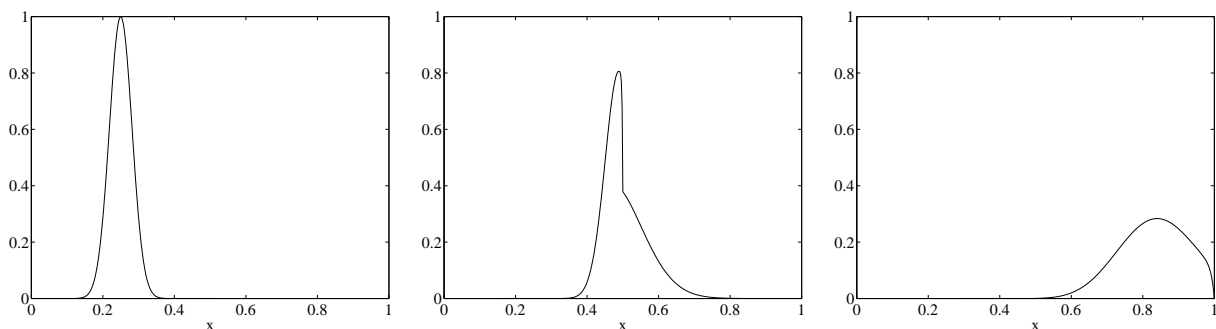


FIGURE 9. From left to right: initial condition and numerical solution at time equal 4 and time equal 7 for Example 2.

*In Figure 10 we illustrate the behavior of the strategy adopted to resolve the time integral. In particular we show (in the left image) the evolution of the parameters  $N_n$  (red dots) and  $N_q$  (black dots) along the time iterations  $n$ . In the right image, we show the gain (in %) when we consider the number of numerical solutions actually stored with the number that would be required without the adopted strategy. As can be seen the number of solutions stored is considerably smaller than the number of numerical solutions (given by  $n$ ). At the final time level we only have stored less than 10% of all the  $n$  numerical solutions.*

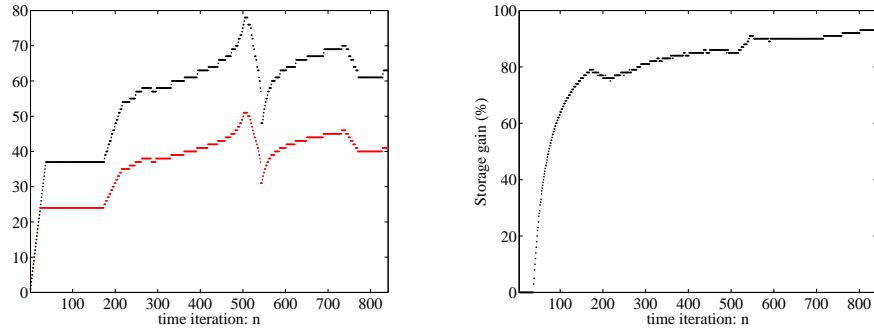


FIGURE 10. In the left: evolution of  $N_n$  (red dots) and  $N_q$  (black dots) over the number of time iterations  $n$ . In the right: evolution of the percentage gain in the number of numerical solutions stored over the number of time iterations  $n$ .

*It is also important to note that the relative maximum difference between the numerical solutions obtained with and without the adopted strategy at the final time level is of the order of  $10^{-6}$ . In terms of computational speed, the proposed strategy is more than three times faster. We expect the speedup to increase significantly as the simulation time increases.*

## Acknowledgments

This work was partially supported by the Centre for Mathematics of the University of Coimbra – UID/MAT/00324/2019, funded by the Portuguese Government through FCT/MEC and co-funded by the European Regional Development Fund through the Partnership Agreement PT2020.

## References

- [1] S. Becker. Transport modeling of skin electroporation and the thermal behavior of the stratum corneum. *International Journal of Thermal Sciences*, 54:48–61, 2012.
- [2] S. Becker, B. Zorec, D. Miklacič, and N. Pavšelj. Transdermal transport pathway creation: electroporation pulse order. *Mathematical Biosciences*, 257:60–68, 2014.
- [3] S.M. Becker. Skin electroporation with passive transdermal transport theory: a review and a suggestion for future numerical model development. *Journal of Heat Transfer*, 133:011011–011011–9, 2010.
- [4] G. Boss and J. Seegmiller. Age-related physiological changes and their clinical significance. *Western Journal of Medicine*, 135:434–440, 1981.
- [5] H. F. Brinson and L. C. Brinson. *Polymer Engineering Science and Viscoelasticity, An Introduction*. Springer, New York, 2008.
- [6] M.L. Crichton, B.C. Donose, X. Chen, A.P. Raphael, H.Huang, and M.A.F. Kendall. The viscoelastic, hyperelastic and scale dependent behaviour of freshly excised individual skin layers. *Biomaterials*, 32:4670–4681, 2011.

- [7] S. Diridollou, V. Vabre, M. Berson, L. Vaillant, D. Black, J.M. Lagarde, J.M. Grégoire, Y. Gall, and F. Patat. Skin ageing: changes of physical properties of human skin in vivo. *International Journal of Cosmetic Science*, 23:353–362, 2001.
- [8] M. Farage, K. Miller, P. Elsner, and H. Maibach. Characteristics of the aging skin. *Advances in Wound Care*, 2:5–10, 2013.
- [9] J.A. Ferreira, P. de Oliveira, P.M. da Silva, and L. Simon. Molecular transport in viscoelastic materials: mechanistic properties and chemical affinities. *SIAM Journal on Applied Mathematics*, 74:1598–1614, 2014.
- [10] J.A. Ferreira, P. de Oliveira, M. Grassi, and G. Romanazzi. Drug release from viscoelastic swelling polymeric platforms. *SIAM Journal on Applied Mathematics*, 78:1378–1401, 2018.
- [11] J.A. Ferreira, P. de Oliveira, and G. Pena. Transdermal iontophoresis - a quantitative and qualitative study. *Computers & Mathematics With Applications*, 74:2231–2242, 2017.
- [12] J.A. Ferreira, M. Grassi, E. Gudiño, and P. de Oliveira. A 3D model for mechanistic control of drug release. *SIAM Journal on Applied Mathematics*, 74:620–633, 2014.
- [13] J.A. Ferreira, M. Grassi, E. Gudiño, and P. de Oliveira. A new look for non-Fickian diffusion. *Applied Mathematical Modelling*, 39:194–204, 2015.
- [14] J.A. Ferreira, G. Pena, and P. de Oliveira. Transdermal iontophoresis - A quantitative and qualitative study. *Computers & Mathematics with Applications*, 74:2231–2242, 2017.
- [15] J.A. Ferreira and L. Pinto. An integro-differential model for non-Fickian tracer transport in porous media: validation and numerical simulation. *Mathematical Methods in the Applied Sciences*, 39:4736–4749, 2016.
- [16] M. Galli, K.S.C. Comley, T.A.V. Shean, and M.L. Oyen. Viscoelastic and poroelastic mechanical characterization of hydrated gels. *Journal of Materials Research*, 24:973–979, 2009.
- [17] S. Ghosal. Fluid mechanics of electroosmotic flow and its effect on band broadening in capillary electrophoresis. *Electrophoresis*, 25:214–228, 2004.
- [18] T. Gratieri and Y.N. Kalia. Mathematical models to describe iontophoretic transport in vitro and in vivo and the effect of current application on the skin barrier. *Advanced Drug Delivery Reviews*, 65:315–329, 2013.
- [19] Y. Hara, Y. Masuda, T. Hirao, and N. Yoshikawa. The relationship between the Young’s modulus of the stratum corneum and age: a pilot study. *Skin Research and Technology*, 19:339–345, 2013.
- [20] W. Hundsdorfer and S.J. Ruuth. IMEX extensions of linear multistep methods with general monotonicity and boundedness properties. *Journal of Computational Physics*, 225:2016–2042., 2007.
- [21] G. Jiang and C.-W. Shu. Efficient implementation of weighted ENO schemes. *Journal of Computational Physics*, 126:202–228, 1996.
- [22] L-Z. Kaestli, A-F. Wasilewski-Rasca, P. Bonnabry, and N. Vogt-Ferrier. Use of transdermal drug formulations in the elderly. *Drugs Aging*, 25:269–280, 2008.
- [23] S. Konda, S. Meier-Davis, B. Cayme, J. Shudo, and H. Maibach. Age-related percutaneous penetration part 1: skin factors. *Skin Therapy Letter*, 17:5, 2012.
- [24] O. Kuwazuru, J. Saothong, and N. Yoshikawa. Mechanical approach to aging and wrinkling of human facial skin based on the multistage buckling theory. *Medical Engineering & Physics*, 30:516–522, 2008.
- [25] X.-D. Liu, S. Osher, and T. Chan. Weighted essentially non-oscillatory schemes. *Journal of Computational Physics*, 115:200–212, 1994.
- [26] A. Peyman, C. Gabriel, E.H. Grant, G. Vermeeren, and L. Martens. Variation of the dielectric properties of tissues with age: the effect on the values of SAR in children when exposed to walkie-talkie devices. *Physics in Medicine and Biology*, 54:227–241, 2009.

- [27] A. Peyman, A.A. Rezazadeh, and C. Gabriel. Changes in the dielectric properties of rat tissue as a function of age at microwave frequencies. *Physics in Medicine and Biology*, 46:1617–1629, 2001.
- [28] R. Pignatello, M. Fresta, and G. Puglisi. Transdermal drug delivery by iontophoresis. I. Fundamentals and theoretical aspects. *Journal of Applied Cosmetology*, 14:59–72, 1996.
- [29] M.J. Pikal. Transport mechanisms in iontophoresis. I. A theoretical model for the effect of electroosmotic flow on flux enhancement in transdermal iontophoresis. *Pharmaceutical Research*, 7:118–126, 1990.
- [30] G. Pontrelli, M. Lauricella, J.A. Ferreira, and G. Pena. Iontophoretic transdermal drug delivery: a multi-layered approach. *Mathematical Medicine and Biology: A Journal of the IMA*, 34:559–576, 2017.
- [31] A.P. Raphael, S.C. Meliga, X. Chen, G.J.P. Fernando, C. Flaim, and M.A.F. Kendall. Depth-resolved characterization of diffusion properties within and across minimally-perturbed skin layers. *Journal of Controlled Release*, 166:87–94, 2013.
- [32] H.S. Ryu, Y.H. Joo, S.O. Kim, K.C. Park, and S.W. Youn. Influence of age and regional differences on skin elasticity as measured by the Cutometer<sup>®</sup>. *Skin Research and Technology*, 14:354–358, 2008.
- [33] C.-W. Shu. High order weighted essentially nonoscillatory schemes for convection dominated problems. *SIAM Review*, 51:82–126, 2009.
- [34] F.H. Silver, J.W. Freeman, and D. DeVore. Viscoelastic properties of human skin and processed dermis. *Skin Research and Technology*, 7:18–23, 2001.
- [35] K. Tojo. Mathematical model of iontophoretic transdermal drug delivery. *Journal of Chemical Engineering of Japan*, 22:512–518, 1989.
- [36] K. Turnheim. When drug therapy gets old: pharmacokinetics and pharmacodynamics in the elderly. *Experimental Gerontology*, 38:843–853, 2003.
- [37] J.M. Waller and H.I. Maibach. Age and skin structure and function, a quantitative approach (I): blood flow, pH, thickness, and ultrasound echogenicity. *Skin Research and Technology*, 11:221–235, 2005.

J.A. FERREIRA

CMUC, DEPARTMENT OF MATHEMATICS, UNIVERSITY OF COIMBRA, PORTUGAL

*E-mail address:* ferreira@mat.uc.pt

P. DE OLIVEIRA

CMUC, DEPARTMENT OF MATHEMATICS, UNIVERSITY OF COIMBRA, PORTUGAL

*E-mail address:* poliveir@mat.uc.pt

L. PINTO

CMUC, DEPARTMENT OF MATHEMATICS, UNIVERSITY OF COIMBRA, PORTUGAL

*E-mail address:* luisp@mat.uc.pt